Long-Range, Photon-Mediated Exciton Hybridization in an All-Organic, One-Dimensional Photonic Crystal

Grant H. Lodden and Russell J. Holmes*

Department of Chemical Engineering and Materials Science, University of Minnesota, Minneapolis, Minnesota 55455, USA

(Received 24 August 2011; published 27 August 2012)

We demonstrate an all-organic, one-dimensional photonic crystal tuned to the regime of strong exciton-photon coupling. The structure consists of a high index of refraction light-absorbing active layer periodically distributed in a low index of refraction nonabsorbing background medium. The strongly coupled state in this structure is shared between multiple active layers separated by distances longer than the wavelength of light in the structure. In order to investigate the potential for long-range energy transfer, photon-mediated exciton hybridization is demonstrated between multiple absorbing species spatially separated in the photonic crystal.

DOI: 10.1103/PhysRevLett.109.096401 PACS numbers: 71.36.+c, 42.70.Jk, 42.70.Qs, 81.05.Fb

Extensive attention has been devoted to the study of semiconductors embedded in optical nanostructures that confine the electromagnetic field and enhance the light-matter interaction [1–11]. When the transition energies of the exciton in the semiconductor and the photon mode are degenerate, an exciton-photon interaction occurs resulting in two distinct regimes of coupling depending on the relative magnitude of the respective transition linewidths [12]. The energy figure of merit separating these regimes is termed the Rabi splitting [12]. When either the photon or exciton linewidth exceeds the Rabi splitting, the regime of weak exciton-photon coupling is reached. This leads to a modification of the emission characteristics of the exciton, both in terms of the spectral shape and excited state lifetime [13,14]. If the photon and exciton transition linewidths are less than the Rabi splitting, the regime of strong coupling is realized. The strongly coupled regime is characterized by a reversible energy exchange between the photon mode and the exciton resulting in the appearance of new eigenstates known as exciton polaritons [8,15]. Exciton polaritons exhibit an energy-in-plane wave vector (or angle of incidence) dispersion consisting of two branches which anticross at the point of degeneracy [16].

Frequently, the regime of strong coupling is accessed by placing the absorbing semiconductor layer at the antinodes of the confined field in an optical microcavity [8,15]. Comparable exciton-photon interactions, however, have also been demonstrated in one-dimensional (1D) photonic crystals [17–20]. These structures are fabricated by periodically arranging the active layers for strong coupling in a uniform nonabsorbing material [21]. The periodicity of the active coupling layers is an integer multiple of half the desired resonant photon wavelength [21]. Multiple reflections at the dielectric-active layer interfaces add constructively to establish the photon modes (or Bragg modes) of the system [22–25]. A large index contrast between the dielectric and active layers is critical in realizing spectrally narrow photon modes and a resolvable exciton-photon coupling [19]. Various active coupling layers including inorganic semiconductors and layered perovskites have been used to observe strong coupling in 1D photonic crystals [17–19,26]. Indeed, polariton amplification was recently demonstrated in a 1D photonic crystal containing quantum wells of InGaAs as the active layers [19]. The regime of strong coupling has also been observed in two-dimensional photonic crystals with semiconductor quantum dots used as the absorbing active material [27,28]. The strongly coupled state in 1D photonic crystal systems is shared among the multiple absorbers of the structure which are often separated by large distances exceeding the wavelength of light. This long-range coupling of semiconductor excited states makes these structures attractive for realizing nonradiative energy transfer over large distances. Thus, the term long range refers to the strong coupling that occurs over the entire thickness of the photonic crystal. A similar effect would be difficult to achieve in a conventional optical microcavity as increasing the cavity length reduces the optical field overlap with the active coupling layer, decreasing the light-exciton coupling.

In this work, an all-organic semiconductor 1D photonic crystal exhibits strong exciton-photon coupling between multiple layers of the active material tetraphenylporphyrin (TPP) spaced in a uniform dielectric background. The large exciton binding energy and absorption coefficient of TPP [Fig. 1(a)] enable the observation of strong coupling in measurements of room temperature reflectivity with a Rabi splitting of (75 ± 7) meV [29–31]. While previous work on all-inorganic 1D photonic crystals has also led to the observation of strong coupling, these studies have not investigated the crucial question of long-range coupling between individual active layers in the structure. Here, by including a second organic semiconductor active material, octaethylporphyrin [OEP, Fig. 1(a)], in the photonic crystal, we demonstrate long-range, photon-mediated hybridization between two different organic semiconductors (TPP and OEP) [32].

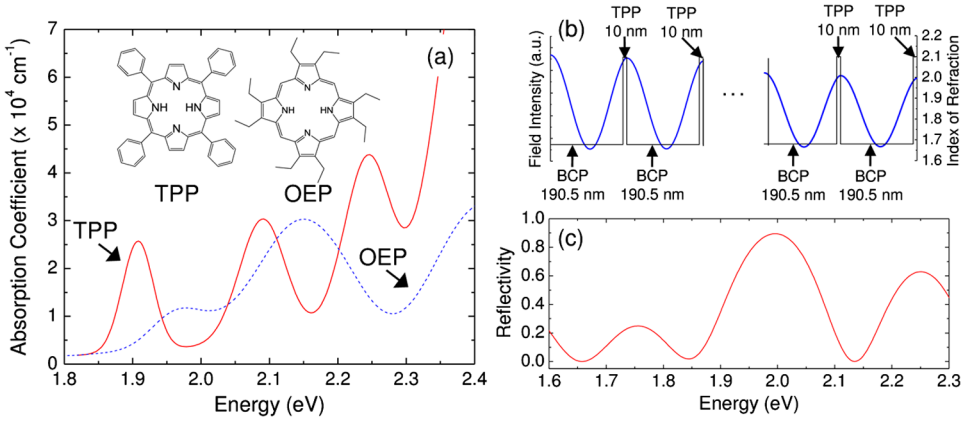

FIG. 1 (color online). (a) The absorption coefficient for 70-nm-thick films of TPP and OEP on glass. (b) Photonic crystal discussed in the text containing eight periods of 190.5 nm BCP and 10 nm TPP. The solid line overlaid over the index of refraction profile is the optical field intensity simulated using a transfer matrix model at an angle of incidence of 27.5° and a wavelength of $\lambda = 650$ nm (1.91 eV). (c) Reflectivity spectrum at 15° simulated for the structure of Fig. 1(b) with a static index of refraction of $n = 2.1$ and an extinction coefficient of $k = 0$ for TPP.

Photonic crystals were constructed by depositing organic thin films onto glass substrates using vacuum thermal sublimation at a pressure of 8×10^{-7} Torr. For photonic crystals containing only a single absorbing active material, the structure consisted of 8 periods of a 190.5-nm-thick layer of the background dielectric material bathocuproine (BCP) and a 10-nm-thick layer of the active material TPP [29,30]. The layer sequence and index of refraction profile for this structure are shown in the inset of Fig. 1(b). A transfer matrix formalism was used to simulate the confined optical field and confirm that the active layers are placed at antinodes [Fig. 1(b)] [33]. The wide energy-gap material BCP was chosen as the background dielectric material in order to prevent parasitic absorption at the energies of interest for strong coupling [34]. Reflectivity measurements were performed using a variable-angle spectroscopic ellipsometer with *s*-polarized light illumination.

In order to characterize the stop band of the photonic crystal, reflectivity spectra were simulated using an optical transfer matrix model with a static index of refraction $n = 2.1$ and an extinction coefficient $k = 0$ for TPP [shown in Fig. 1(c)]. The structure exhibits a 0.27 eV wide photonic band gap centered at ~2.0 eV with $Q = 17$ corresponding to a photon Bragg mode FWHM linewidth of 68 meV. A single, 10-nm-thick active layer of TPP embedded within a photonic crystal was confirmed via optical transfer matrix simulations to not be sufficiently absorptive to reach the regime of strong coupling. Hence, the observation of a splitting using the structure shown in Fig. 1(b) would already suggest that the coupling occurs among multiple active layers.

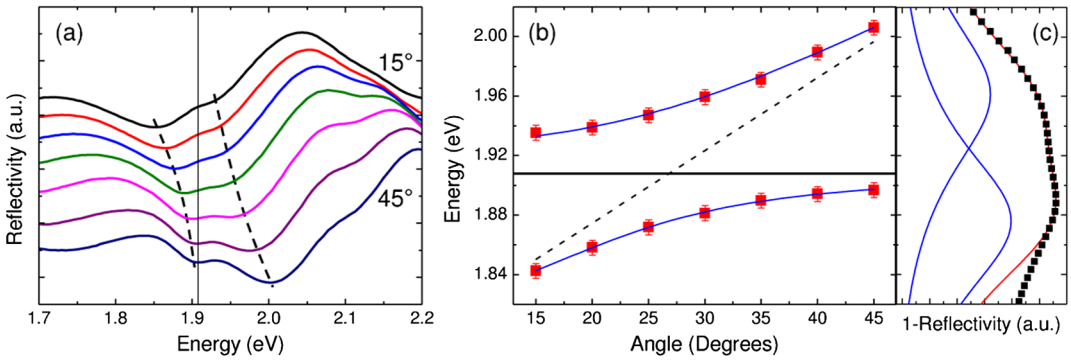

FIG. 2 (color online). (a) Angle-resolved reflectivity and the corresponding dispersion relation (b) collected under *s*-polarized light illumination for the structure in Fig. 1(b). In part (a) the vertical solid line denotes the uncoupled exciton resonance of interest while the broken lines indicate the position of strongly coupled features. In part (b), the horizontal solid line designates the uncoupled exciton resonance, the broken line is the simulated uncoupled photon dispersion, and the solid lines are dispersion curves obtained from a damped two-branch coupled oscillator model. (c) Multipeak fitting for the reflectivity spectrum of Fig. 2(a) collected at an angle of 30°. The spectrum is deconvoluted by multipeak fitting with two Lorentzian peaks representing the lower and upper polariton branches.

The photonic crystal of Fig. 1(b) was tuned to overlap with the excitonic transition of TPP at 1.908 eV [Fig. 1(a)]. Angle-resolved reflectivity spectra for the photonic crystal of Fig. 1(b) are shown in Fig. 2(a). Two spectral features clearly anticross around the uncoupled excitonic resonance of TPP, indicating strong coupling between an optical mode of the photonic crystal and the excitonic transition. A third feature observed at high energy (> 2.05 eV) results from the hybridization of the resonant photon mode with both the 1.908 and 2.091 eV excitonic resonances of TPP. The additional feature observed at low energy (< 1.85 eV) is a lower-order mode of the photonic crystal.

The reflectivity spectra of Fig. 2(a) were multipeak fit to construct a dispersion relation for the exciton-polariton resonances [Fig. 2(b)]. Figure 2(c) shows an example of peak deconvolution for a reflectivity spectrum collected at an angle of incidence of 40° for the structure of Fig. 1(b). The experimental dispersion curve is in good agreement with a damped two-branch coupled oscillator model [Fig. 2(b), solid lines] with fixed parameters that are separately determined. A Rabi splitting of (75 ± 7) meV was calculated as the minimum energetic separation between the upper and lower branches. The photon dispersion [Fig. 2(b)] and linewidth (FWHM = 72 meV) of the photonic crystal were determined via an optical transfer matrix formalism with no free parameters as all layer thicknesses and optical constants for the organic materials were separately measured. The TPP exciton linewidth (FWHM = 69 meV) and energy (1.908 eV) were determined from the absorption spectrum of Fig. 1(a).

For the hybridized structure that contains two absorbing species [Fig. 3(a)], the layer stack consisted of 4 periods of a 160.5-nm-thick layer of BCP and a 20-nm-thick layer of TPP, followed by 4 periods of a 90.5-nm-thick layer of BCP and a 80-nm-thick layer of OEP. In this structure, both TPP and OEP serve as the active layers for strong coupling. Transfer matrix simulations were again used to ensure maximum overlap between the optical field and each of the active layers [Fig. 3(a)] [33]. The absorption coefficient of OEP is roughly a factor of 2 smaller than that of TPP [Fig. 1(a)]. Since the Rabi splitting in strongly coupled organic semiconductor microcavities increases with active layer absorption [31], the total layer thickness of OEP in the structure is made considerably thicker than that of TPP in order to realize a comparable exciton-photon interaction. By including a second active material, multiple excitonic transitions in the photonic crystal are hybridized via their common interaction with the photon mode. The periods containing TPP and the periods containing OEP are located at opposite ends of the structure of Fig. 3(a). Since the optical excitation is through the periods containing TPP, this arrangement permits the spatial extent of strong coupling to be studied as coupling to OEP will only occur if substantial optical field intensity is present throughout the structure.

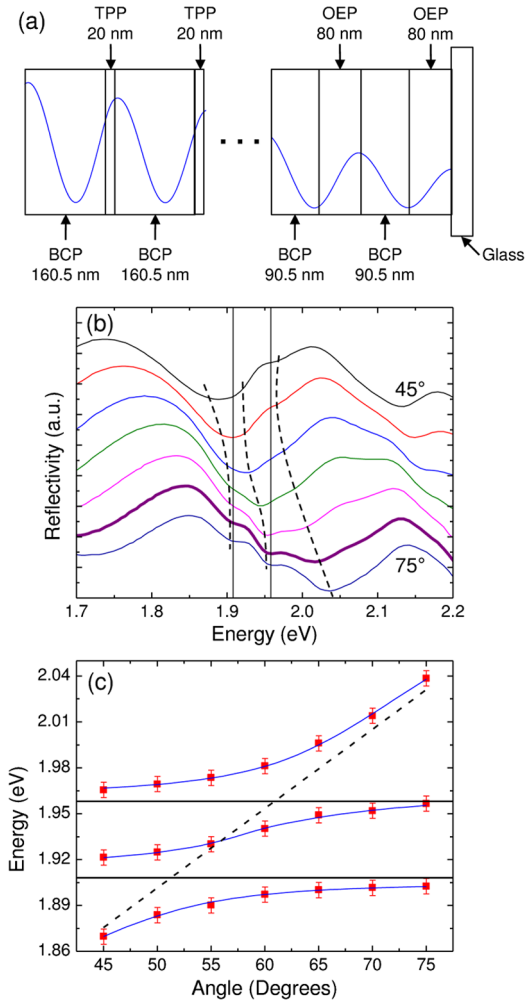

FIG. 3 (color online). (a) Photonic crystal used to examine photon-mediated exciton hybridization. The structure consists of 4 periods of 160.5 nm BCP/20 nm TPP followed by 4 periods of 90.5 nm BCP/80 nm OEP. The solid line is a simulated optical field intensity profile at 70° and a photon wavelength of $\lambda = 642$ nm (1.93 eV). (b) Angle-resolved reflectivity collected under *s*-polarized light illumination and (c) the corresponding dispersion relation. In (b), the reflectivity spectrum collected at 70° (bold) exhibits three clear features confirming photon-mediated hybridization between the excitons of TPP and OEP and the photon mode. The vertical solid lines denote the uncoupled exciton resonances of interest while the broken lines indicate the position of strongly coupled features. In (c), the solid horizontal lines denote the position of the uncoupled exciton resonances, the broken line is a simulated uncoupled photon dispersion curve and the solid lines are dispersion curves obtained from a damped three-branch coupled oscillator model.

Figure 3(b) shows angle-resolved reflectivity for the photonic crystal of Fig. 3(a) which contains two active materials, namely, TPP and OEP. Three prominent features, particularly at an angle of 70°, are observed due to the photon-mediated hybridization of the excitonic transitions of TPP at 1.908 eV and that of OEP at 1.958 eV with the optical mode of the photonic crystal.

The two additional spectral features observed at high energy (> 2.05 eV) are attributed to a coupling between a higher order mode of the photonic crystal and the TPP excitonic resonance at 2.09 eV while the additional spectral feature observed at low (< 1.85 eV) energy is a lower-order mode of the photonic crystal. Multipeak fitting was performed on the reflectivity spectra to extract the position of each feature and construct a dispersion curve [Fig. 3(c)]. Branch splittings of (40 ± 7) and (41 ± 7) meV are determined as the minimum energetic separation between the middle and lower branches (TPP exciton), and the upper and middle branches (OEP exciton), respectively. As in the case of the photonic crystal of Fig. 1(b), a transfer matrix simulation was used to determine the photon dispersion and linewidth (FWHM $= 39$ meV) of the photonic crystal. The aforementioned parameters and exciton linewidths of TPP (FWHM $= 69$ meV) and OEP (FWHM $= 70$ meV) as determined from Fig. 1(a) were set as fixed parameters in a damped three-branch coupled oscillator model. Good agreement is obtained in Fig. 3(c) between experiment (symbols) and the damped three-branch coupled oscillator model (solid lines).

Figure 4 shows the mixing coefficients extracted from the three-body coupled oscillator model plotted versus angle for each branch of the dispersion relation in Fig. 3(c) [19]. The lower polariton branch exhibits symmetrically varying degrees of photon and TPP exciton character. The middle polariton branch demonstrates significant mixing between the photon, the TPP exciton, and the OEP exciton. Maximum mixing occurs at an angle of $\sim 55°$, where the middle branch polariton character is equal parts TPP and OEP exciton ($\sim 42\%$) and $\sim 16\%$ photon. Consistent with previous reports of photon-mediated hybridization, the large branch splittings lead to a gradual middle branch dispersion with angle and a small photon contribution to the overall

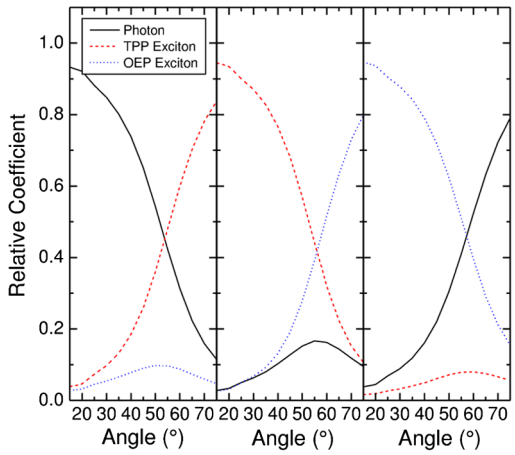

FIG. 4 (color online). Mixing coefficients extracted from the dispersion relation of Fig. 3(c) for the lower (a), middle (b), and upper (c) branches. The middle branch demonstrates the most significant mixing between the TPP and OEP excitons and the photon mode of interest.

character of the middle branch [32]. The upper branch consists mainly of OEP exciton and photon character with some mixing of the TPP exciton occurring at large angles. The presence of hybrid exciton-polariton states in the structure confirms that long-range strong coupling is present as the resonant photon mode clearly samples the entire structure.

In examining the reflectivity spectra obtained from the structures of Figs. 1(b) and 3(a), it is interesting to note that in both cases, the observed Rabi splittings are comparable in magnitude to the respective exciton and photon linewidths. Broad exciton linewidths are frequently observed in disordered organic semiconductors, and have been previously discussed in the context of polariton coherence. Work by Agranovich *et al.* [35] has suggested that depending on their energy and in-plane wave vector, polaritons in such systems can exhibit either coherent or incoherent behavior. For the photonic crystal structures investigated here, a closer examination of polariton coherence could reveal a similar behavior.

In conclusion, an all-organic 1D photonic crystal is demonstrated that permits the observation of strong exciton-photon coupling at room temperature with Rabi splittings that are an order of magnitude larger than those observed in inorganic analogs [18]. The long-range character of the coupling is confirmed through the observation of photon-mediated exciton hybridization between two different absorbers that are spatially separated in the structure. While in this work the separation between absorbers is 90.5 nm, the extended nature of the photon mode will permit hybridization to be observed over considerably larger distances as well. The unique attributes of all-organic photonic crystals tuned to the regime of strong exciton-photon coupling make this an interesting platform for the examination of energy transfer between spatially separated excited states. Additionally, these structures could offer new opportunities for the development of polariton-based devices.

Primary support for this work was received from the NSF MRSEC Program under Grant No. DMR-0819885. Part of this work was carried out in the University of Minnesota Characterization Facility, which has received funding from the NSF through the MRSEC, ERC, and MRI programs.

*rholmes@umn.edu

[1] H. Benisty, J.-M. Gerard, R. Houdré, J. Rarity, and C. Weisbuch, *Confined Photon Systems: Fundamentals and Applications* (Springer, Berlin, 1998).

[2] E. Burnstein and C. Weisbuch, *Confined Electrons and Photons: New Physics and Applications* (Plenum Press, New York, 1995).

[3] Y. Yamamoto, F. Tassone, and H. Cao, *Semiconductor Cavity Quantum Electrodynamics* (Springer-Verlag, New York, 2000).

[4] H. Benisty, H. De Neve, and C. Weisbuch, IEEE J. Quantum Electron. **34**, 1612 (1998).
[5] A. Yariv, *Optical Electronics in Modern Communications* (Oxford University Press, New York, 1997).
[6] T. Yoshie, A. Scherer, J. Hendrickson, G. Khitrova, H. Gibbs, G. Rupper, C. Ell, O. Shchekin, and D. Deppe, Nature (London) **432**, 200 (2004).
[7] J. Reithmaier, G. Sek, A. Loffler, C. Hofmann, S. Kuhn, S. Reitzenstein, L. Keldysh, V. Kulakovskii, T. Reinecke, and A. Forchel, Nature (London) **432**, 197 (2004).
[8] M. S. Skolnick, T. A. Fisher, and D. M. Whittaker, Semicond. Sci. Technol. **13**, 645 (1998).
[9] M. S. Skolnick, A. I. Tartakovskii, R. Butte, D. M. Whittaker, and R. M. Stevenson, IEEE J. Sel. Top. Quantum Electron. **8**, 1060 (2002).
[10] D. Englund, A. Faraon, I. Fushman, N. Stoltz, P. Petroff, and J. Vuckovic, Nature (London) **450**, 857 (2007).
[11] D. Englund, D. Fattal, E. Waks, G. Solomon, B. Zhang, T. Nakaoka, Y. Arakawa, Y. Yamamoto, and J. Vuckovic, Phys. Rev. Lett. **95**, 013904 (2005).
[12] R. Houdré, R. P. Stanley, U. Oesterle, M. Ilegems, and C. Weisbuch, Phys. Rev. B **49**, 16 761 (1994).
[13] H. Yokoyama, K. Nishi, T. Anan, H. Yamada, S. D. Brorson, and E. P. Ippen, Appl. Phys. Lett. **57**, 2814 (1990).
[14] R. H. Jordan, L. J. Rothberg, A. Dodabalapur, and R. E. Slusher, Appl. Phys. Lett. **69**, 1997 (1996).
[15] C. Weisbuch, M. Nishioka, A. Ishikawa, and Y. Arakawa, Phys. Rev. Lett. **69**, 3314 (1992).
[16] R. Houdré, C. Weisbuch, R. P. Stanley, U. Oesterle, P. Pellandini, and M. Ilegems, Phys. Rev. Lett. **73**, 2043 (1994).
[17] M. Hübner, J. P. Prineas, C. Ell, P. Brick, E. S. Lee, G. Khitrova, H. M. Gibbs, and S. W. Koch, Phys. Rev. Lett. **83**, 2841 (1999).
[18] D. Goldberg, L. I. Deych, A. A. Lisyansky, Z. Shi, V. M. Menon, V. Tokranov, M. Yakimov, and S. Oktyabrsky, Nature Photon. **3**, 662 (2009).
[19] A. Askitopoulos, L. Mouchliadis, I. Iorsh, G. Christmann, J. J. Baumberg, M. A. Kaliteevski, Z. Hatzopoulos, and P. G. Savvidis, Phys. Rev. Lett. **106**, 076401 (2011).
[20] F. Biancalana, L. Mouchliadis, C. Creatore, S. Osborne, and W. Langbein, Phys. Rev. B **80**, 121306 (2009).
[21] R. H. Dicke, Phys. Rev. **93**, 99 (1954).
[22] M. V. Erementchouk, L. I. Deych, and A. A. Lisyansky, Phys. Rev. B **71**, 235335 (2005).
[23] M. V. Erementchouk, L. I. Deych, and A. A. Lisyansky, Phys. Rev. B **73**, 115321 (2006).
[24] A. Yu. Sivachenko, M. E. Raikh, and Z. V. Vardeny, Phys. Rev. A **64**, 013809 (2001).
[25] S. Nojima, Phys. Rev. B **59**, 5662 (1999).
[26] K. Sumioka, H. Nagahama, and T. Tsutsui, Appl. Phys. Lett. **78**, 1328 (2001).
[27] K. Hennessy, A. Badolato, M. Winger, D. Gerace, M. Atatuere, S. Gulde, S. Faelt, E. L. Hu, and A. Imamoglu, Nature (London) **445**, 896 (2007).
[28] D. Englund, A. Majumdar, A. Faraon, M. Toishi, N. Stoltz, P. Petroff, and J. Vučković, Phys. Rev. Lett. **104**, 073904 (2010).
[29] R. J. Holmes and S. R. Forrest, Phys. Rev. B **71**, 235203 (2005).
[30] G. H. Lodden and R. J. Holmes, Phys. Rev. B **83**, 075301 (2011).
[31] D. G. Lidzey, D. D. C. Bradley, M. S. Skolnick, T. Virgili, S. Walker, and D. M. Whittaker, Nature (London) **395**, 53 (1998).
[32] D. G. Lidzey, D. D. C. Bradley, A. Armitage, S. Walker, and M. S. Skolnick, Science **288**, 1620 (2000).
[33] L. A. A. Pettersson, L. S. Roman, and O. Inganas, J. Appl. Phys. **86**, 487 (1999).
[34] I. Hill and A. Kahn, J. Appl. Phys. **86**, 4515 (1999).
[35] V. M. Agranovich, M. Litinskaia, and D. G. Lidzey, Phys. Rev. B **67**, 085311 (2003).